Dicer accumulates in cytoplasmic foci upon alphavirus infection and plays a proviral role in *Myotis myotis* bat cells

Léa Gaucherand*, Hugo Marie*, Julie Cremaschi, Sébastien Pfeffer‡

Université de Strasbourg, Architecture et Réactivité de l'ARN, Institut de Biologie Moléculaire et Cellulaire du CNRS, 67000 Strasbourg, France

* These authors contributed equally and should be considered as co-first authors

‡ To whom correspondence should be addressed: s.pfeffer@ibmc-cnrs.unistra.fr

Abstract

Bats are reservoirs for many viruses that frequently cause epidemics in humans and animals. It is thus critical to better understand their immune system and mechanisms of antiviral immunity. Despite an increasing number of studies, much is still unknown about the molecular mechanisms that govern bat-virus interactions, especially given the large diversity of bat species. Dicer is a conserved ribonuclease with multiple activities that can modulate antiviral immunity, including the detection of viral RNA as part of the RNA interference (RNAi) pathway, the maturation of micro RNAs, and the direct inhibition of innate immunity in mouse and human cells. In view of these complex activities of Dicer, we tested its antiviral activity in *Myotis myotis* nasal epithelial cells. Surprisingly, we did not see strong evidence of RNAi in these cells, but instead saw a proviral effect of Dicer for two alphaviruses, Sindbis and Semliki forest virus. We also observed a striking relocalization of Dicer to cytoplasmic foci upon infection with these viruses, which did not occur in the several human cell lines we tested. These foci contained dsRNA and viral plus strand RNA, suggesting that they are sites of viral replication. Finally, we found that factors specific to *M. myotis* cells are needed for Dicer relocalization. Overall, we propose that Dicer can play different roles in different bat species and/or cell types, and is being repurposed by alphaviruses to promote viral replication.

Introduction

Bats are unique mammals in many aspects, such as their ability to fly and their high longevity relative to their body size (Gonzalez & Banerjee, 2022). They belong to the order Chiroptera, which can be divided into two suborders that diverged over 50 million years ago (Lei & Dong, 2016). More than 1400 different species of bats have been identified so far, accounting for 20% of all mammals (Burgin *et al*, 2018). Importantly, bats are reservoirs for many viruses that can spillover into humans, either directly or through an intermediate host, such as Marburg virus, Hendra and Nipah virus, Middle East respiratory syndrome coronavirus (MERS-CoV), severe acute respiratory syndrome coronavirus (SARS-CoV) and likely SARS-CoV-2 (Halpin *et al*, 2000; Li *et al*, 2005; Memish *et al*, 2013; Moratelli & Calisher, 2015; Chua *et al*, 2002; Yob *et al*, 2001; Towner *et al*, 2007). Interestingly, while these viruses can be very pathogenic to humans and other animals, most of the studied bats so far show little to no clinical symptoms, whether they were naturally or experimentally infected (Gonzalez &

52 Banerjee, 2022; Pei *et al*, 2024). An increasing number of studies are highlighting the
53 role of the bat innate immune system in this apparent tolerance to viruses.
54 The type I and III interferon (IFN) pathways are the main first lines of defense
55 against viruses in mammals. In this pathway, sensing of viral nucleic acids by pattern
56 recognition receptors (PRRs) leads to the expression and secretion of type I and III
57 IFN cytokines. These cytokines are then sensed by cells in an autocrine and paracrine
58 fashion, leading to the expression of interferon stimulated genes (ISGs) that can
59 actively fight the infection (Pichlmair & Reis e Sousa, 2007). The IFN pathway is
60 present and active in bats, but differences have been reported compared to humans,
61 as well as between different bat species. These include a dampening of the response
62 to DNA sensing, as well as differences in the baseline expression and temporal
63 regulation of some IFNs and ISGs (Irving *et al*, 2021; Banerjee *et al*, 2020; Clayton &
64 Munir, 2020). In contrast, invertebrates and plants mostly rely on the RNA interference
65 (RNAi) pathway to fight viral infections. In antiviral RNAi, viral double-stranded
66 (ds)RNAs are sensed and cleaved into small interfering (si)RNAs by a Dicer or Dicer-
67 like ribonuclease, then loaded into a protein of the Argonaute family to target and
68 degrade complementary viral RNAs (Guo *et al*, 2019). Interestingly, two recent studies
69 have reported enhanced antiviral activity of Dicer through the RNAi pathway in the
70 *Pteropus alecto* kidney (PaKi) cell line infected with SINV, an NS1 deletion mutant
71 strain of infuenza A virus and a B2 deletion mutant strain of Nodamura virus, and in
72 the *Tadarida brasiliensis* lung (TBLU) cell line infected with SARS-CoV-2 (Dai *et al*,
73 2024; Owolabi *et al*, 2025). The first study also proposed that viral dsRNA cleavage
74 by Dicer limits the recognition of dsRNA by PRRs and thus the activation of the IFN
75 response in *P. alecto*, thereby suggesting a role for Dicer in bat viral tolerance (Dai *et*
76 *al*, 2024).
77 Dicer is well known for its essential role in the maturation of most micro (mi)RNAs,
78 key regulators of gene expression (Bartel, 2018). In mammals, the same Dicer protein
79 can generate both miRNAs and siRNAs of 22 nucleotides (nt) thanks to its regulatory
80 cofactors transactivation response element RNA-binding protein (TRBP) and Protein
81 ACTivator of the interferon-induced protein kinase (PACT) (Lee *et al*, 2013). However,
82 the antiviral activity of Dicer through the RNAi pathway is controversial and appears
83 to be cell-type and context-dependent in human and mouse cells (Cullen *et al*, 2013).
84 Indeed, Dicer isoforms with increased RNAi activity have been identified in human and
85 mouse stem cells (Poirier *et al*, 2021), and in mouse oocytes (Flemr *et al*, 2013). While

86 the former appears to have some antiviral properties against viruses such as Zika and
87 SARS-CoV-2 (Poirier *et al*, 2021), the mouse oocyte specific one does not confer an
88 antiviral phenotype when artificially expressed ubiquitously (Kulmann *et al*, 2025). One
89 important reason for the reduced antiviral activity of full-length Dicer is the existence
90 of a regulatory crosstalk between the IFN and RNAi pathways (Baldaccini & Pfeffer,
91 2021; Gaucherand *et al*, 2024; Maillard *et al*, 2019). Human Dicer is inhibited by the
92 PRR LGP2 (laboratory of genetics and physiology 2 / DexH box polypeptide 58) (van
93 der Veen *et al*, 2018). Moreover, inactivating the IFN pathway in differentiated mouse
94 cells unmasks long dsRNA processing by Dicer (Maillard *et al*, 2016). Conversely,
95 Dicer represses IFN and the ISG protein kinase R (PKR) activity in mouse embryonic
96 stem cells transfected with double stranded RNA (Gurung *et al*, 2021). In addition, we
97 recently showed that human Dicer interacts with PKR *via* its helicase domain and
98 regulates innate immune activation during Sindbis virus (SINV) infection (Montavon *et*
99 *al*, 2021; Baldaccini *et al*, 2024).
100 Overall, Dicer could modulate antiviral activity through its role in the RNAi pathway,
101 but also by maturing miRNAs that can affect viral infection, by directly regulating innate
102 immune activation, and potentially through other still unknown mechanisms. How
103 these multiple complex activities of Dicer could contribute to antiviral activity and viral
104 tolerance in different bat species is still poorly understood. This prompted us to
105 investigate the antiviral activity of Dicer in the greater mouse-eared bat (*Myotis*
106 *myotis*), a European microbat from the *Vespertilionidae* family. Unexpectedly,
107 expressing *M. myotis* Dicer in human Dicer knock out cells did not protect from viral
108 infection. Instead, we saw a proviral role of Dicer in *M. myotis* nasal epithelial cells
109 upon infection with two different alphaviruses, with no clear evidence of antiviral RNAi
110 activity. Interestingly, Dicer relocalizes to large cytoplasmic foci upon infection with
111 these viruses in *M. myotis* nasal epithelial cells but not in human cells. We find that
112 these foci are likely viral factories and that *M. myotis* cell-specific factors are required
113 for Dicer relocalization. Overall, we propose that the activity of bat Dicer is context-
114 dependent and could be used by some viruses like SINV in *M. myotis* cells to promote
115 viral replication.
116
117 **Results**
118 Expressing *M. myotis* Dicer in NoDice cells does not protect from SINV and VSV
119 infection

120 Since *P. alecto* and *T. brasiliensis* Dicer were found to be antiviral against a few viruses
121 (Dai *et al*, 2024; Owolabi *et al*, 2025), we tested the antiviral activity of *M. myotis* Dicer.
122 We cloned Dicer from *M. myotis* cells (hereafter referred to as mmDicer) and
123 expressed it with an HA tag in human embryonic kidney (HEK) 293T cells knock-out
124 for Dicer (NoDice cells (Bogerd *et al*, 2014)). As controls, we also expressed an HA-
125 tagged catalytically inactive mutant (amino acid changes E1562A and E1819A)
126 version of *M. myotis* Dicer (hereafter referred to as mmDicer CM), HA-tagged human
127 Dicer (hDicer), or an empty vector (Empty). Efficient expression of the different Dicer
128 constructs was checked by western blot (**Fig. 1A**). Expressing mmDicer but not
129 mmDicer CM also rescued maturation of the human miRNA miR-16 (**Fig. 1B**). These
130 results suggested that mmDicer is indeed expressed and active in NoDice cells. We
131 then tested its antiviral activity against a SINV that expresses GFP (SINV-GFP) (López
132 *et al*, 2020). Expressing mmDicer did not lead to a significant decrease in SINV-GFP
133 titers, RNA and protein levels compared to the empty vector control, hDicer or
134 mmDicer CM (**Fig. 1C-E**), suggesting that mmDicer is not particularly antiviral against
135 SINV in this context. We also tested a different virus, the rhabdovirus vesicular
136 stomatitis virus expressing GFP (VSV-GFP), and again saw no antiviral activity of
137 mmDicer (**Fig. 1F**). Overall, these results suggest that expressing mmDicer in a
138 human cell line does not protect against SINV and VSV infection.
139
140 <u>Dicer is proviral for two alphaviruses in *M. myotis* nasal epithelial cells</u>
141 To determine whether mmDicer displays antiviral activity in *M. myotis* cells, we used a
142 pool of multiple siRNAs at low concentrations to knock down Dicer in a SV40
143 transformed *M. myotis* nasal epithelial cell line (He *et al*, 2014b). This technique allows
144 for efficient knock down (**Fig. 2A**) while limiting off-target effects. We then infected
145 these cells with SINV-GFP and VSV-GFP. Interestingly, we saw that knocking down
146 Dicer actually reduced SINV-GFP replication, as seen by a decrease in GFP+ cells
147 over time (**Fig. 2B**). At 24h, we also saw a decrease in SINV-GFP titers, in GFP protein
148 levels and in SINV RNA levels (**Fig. 2C-E**). To test whether the proviral effect of Dicer
149 could be recapitulated with another alphavirus, we infected our *M. myotis* cell line with
150 Semliki forest virus (SFV). Similar to SINV infection, knocking down Dicer decreased
151 SFV titers and RNA levels at 24 hours post infection (**Fig. 2F-G**). In contrast, Dicer
152 knock down had an antiviral effect against VSV-GFP infection at the RNA and protein
153 levels, but no difference in titers was found (**Fig. 2H-J**). Overall, our results suggest

154 that Dicer plays a proviral role for SINV and SFV but not VSV infection in *M. myotis*
155 nasal epithelial cells.
156
157 *M. myotis* nasal epithelial cells only display a mild RNAi signature
158 Since *P. Alecto* and *T. brasiliensis* Dicer have enhanced antiviral RNAi activity, we
159 wondered whether there was any evidence of antiviral RNAi activity in our *M. myotis*
160 nasal epithelial cell line. We infected these cells with SINV-GFP and VSV-GFP, then
161 sequenced small RNAs isolated from these cells. As control, we followed the same
162 procedure with HEK293T cells, which we have previously showed display a weak
163 RNAi signature against SINV-GFP (Girardi *et al*, 2013). Consistent with the lack of
164 antiviral activity of mmDicer against SINV-GFP (**Fig. 1-2**), we did not observe a
165 stronger RNAi signature against SINV-GFP in *M. myotis* cells than in HEK293T cells
166 (**Fig. 3** and **S1**). This was also true for VSV-GFP (**Fig. 3** and **S1**), even though Dicer
167 seemed to interfere with VSV-GFP at the RNA and protein level in *M. myotis* cells (**Fig.**
168 **2**). In both HEK293T and *M. myotis* cells, only a very low percentage of reads aligned
169 to the SINV-GFP genome, and even lower to the VSV-GFP genome (**Fig. 3A**).
170 Focusing on the SINV-GFP reads, while they showed an enrichment at 22nt on both
171 strands in HEK293T cells, there was an enrichment of smaller size RNAs on the
172 positive strand in the *M. myotis* cells, suggesting the presence of viral RNA
173 degradation products (**Fig. 3B** and **S1A**). The same enrichment for smaller size RNAs
174 on the positive strand could be seen for VSV-GFP reads in *M. myotis* cells, while
175 almost no reads aligned to the VSV-GFP genome in HEK293T cells (**Fig. 3B** and **S1A**).
176 The few viral reads that were 22nt long did display typical RNAi characteristics in both
177 cell lines, as they aligned to both strands and throughout the viral genome (**Fig. 3C**
178 and **S1B**). In both cell lines there was also an enrichment for paired positive and
179 negative sense SINV-GFP reads that overlapped with a 2nt overhang, a signature of
180 Dicer cleavage as part of the RNAi pathway (**Fig. 3D** and **S1C**), although that was not
181 the case for VSV-GFP reads. However, the very low total number of viral reads of 22nt
182 in both cell lines argues against a strong antiviral RNAi activity of mmDicer in *M. myotis*
183 nasal epithelial cells against SINV and VSV. Altogether, our results indicate that
184 mmDicer does not appear to have increased RNAi activity in *M. myotis* nasal epithelial
185 cells.
186

187 Dicer relocalizes to cytoplasmic foci upon SINV infection in *M. myotis* nasal epithelial
188 cells
189 To try to understand how mmDicer could play a proviral role in *M. myotis* nasal
190 epithelial cells, we looked at the subcellular localization of Dicer upon SINV infection.
191 In mock conditions, mmDicer exhibited a diffuse cytoplasmic localization, but
192 interestingly upon WT SINV infection we saw a striking relocalization of Dicer into
193 discrete cytoplasmic foci in *M. myotis* nasal epithelial cells. This relocalization could
194 already be noticed at 8h (**Fig. 4A**) and was still apparent at 24h (**Fig. 4B**). There was
195 no significant difference in both the number and size distribution of Dicer foci between
196 8h and 24h, although there was a small trend towards a decrease in the number of
197 Dicer foci per cell (**Fig. 4C**). Importantly, we did not see any shift in Dicer localization
198 upon SINV infection for HEK293T cells (**Fig. 4A-B**), as well as for the two other human
199 cell lines we tested, human lung epithelial carcinoma A549 cells and human
200 hepatocyte-derived carcinoma Huh7 cells (**Fig. S2A**). Overall, our results suggest a
201 singular activity of Dicer during SINV infection in *M. myotis* nasal epithelial cells that
202 leads to the relocalization of Dicer in large cytoplasmic foci, but that does not appear
203 to occur in human cells.
204
205 Dicer likely relocalizes to alphavirus viral factories in *M. myotis* nasal epithelial cells
206 SINV infected cells are known to accumulate large quantities of double stranded
207 (ds)RNA in the cytoplasm as a result of replication (Griffin, 2007). Since dsRNA is the
208 primary substrate of Dicer, we wondered if Dicer clustered around dsRNA in SINV
209 infected cells. We infected *M. myotis* nasal epithelial cells with SINV and measured
210 the co-localization of Dicer and dsRNA by confocal microscopy, using J2 antibodies
211 that recognize dsRNAs longer than 40bp (Richardson *et al*, 2010). We saw that many
212 of the Dicer foci co-localized with dsRNA in SINV infected cells (**Fig. 5A**), with a high
213 Pearson correlation coefficient across multiple experiments (**Fig. 5B**), suggesting that
214 Dicer forms foci in close proximity to dsRNA in *M. myotis* cells. As control, we could
215 also see dsRNA accumulating in SINV infected HEK293T, A549 and Huh7 cells but
216 Dicer staining remained diffuse and did not co-localize with dsRNA (**Fig. 5A-B, Fig.
217 S2A**). Importantly, infection with the other alphavirus SFV also led to Dicer foci that
218 co-localized with dsRNA (**Fig. 5A-B**). In contrast, infection with WT VSV is known to
219 not accumulate dsRNA by J2 staining (Weber *et al*, 2006). And indeed, we did not
220 detect dsRNA and there was no relocalization of Dicer upon infection in *M. myotis* cells

221 (**Fig. S2B**). These results suggest that Dicer does not form large foci for every viral
222 infection but its relocalization may be specific to alphaviruses or linked to dsRNA
223 accessibility. dsRNA is often formed during viral replication, we thus wondered if Dicer
224 was present at sites of SINV replication. Since J2 antibodies cannot distinguish
225 between dsRNA of viral origin or originating from the host, we carried out fluorescence
226 *in situ* hybridization (FISH) to specifically stain for SINV plus strand RNA. As expected,
227 we saw discreet foci showing the accumulation of SINV RNA, likely at sites of viral
228 replication, in both HEK293T cells and *M. myotis* nasal epithelial cells (**Fig. 5C**). Again,
229 Dicer stayed diffuse upon infection in HEK293T cells. Importantly, the Dicer foci
230 matched the SINV plus strand RNA foci in *M. myotis* cells (**Fig. 5C**). Altogether, our
231 results argue for the recruitment of Dicer to sites of SINV viral replication.
232
233 <u>*M. myotis* Dicer alone is not sufficient for relocalization in NoDice cells</u>
234 Finally, we wondered if there was something inherently special about mmDicer that
235 triggered its relocalization upon SINV infection. To test this, we went back to our
236 human NoDice cells expressing mmDicer (**Fig. 1**). Immunoprecipitating mmDicer in
237 these cells showed that mmDicer still interacted with known hDicer interactors such
238 as PACT and TRBP in mock conditions, as well as PKR and ADAR1, which we
239 previously showed interact with hDicer during SINV infection (Montavon *et al*, 2021)
240 (**Fig. 6A**). As expected, while J2 staining showed discrete foci characteristic of SINV
241 infection, hDicer stayed diffuse throughout the cytoplasm (**Fig. 6B**). Importantly, there
242 was also no relocalization of mmDicer upon SINV infection (**Fig. 6B**). These results
243 suggest that mmDicer alone is not sufficient to form large foci, and that factors specific
244 to *M. myotis* nasal epithelial cells are required for relocalization.
245
246 **Discussion**
247 Recent studies have highlighted a role for Dicer in bat antiviral immunity and tolerance
248 to viruses through RNAi in two different bat species, *P. alecto* and *T. brasiliensis* (Dai
249 *et al*, 2024; Owolabi *et al*, 2025). In this study, we set out to characterize the antiviral
250 activity of Dicer in *M. myotis* nasal epithelial cells. Interestingly, mmDicer did not
251 protect from SINV and VSV infection when expressed in a human Dicer knock out cell
252 line (**Fig. 1**). Moreover, knocking down Dicer in *M. myotis* nasal epithelial cells led to
253 a decrease in SINV and SFV infection, while results were more mitigated with VSV
254 (**Fig. 2**). Consistent with these results, we did not find a strong antiviral RNAi signature

255 when analyzing the viral small RNA profiles of SINV and VSV infected *M. myotis* nasal
256 epithelial cells (**Fig. 3** and **S1**). However, we did observe a striking relocalization of
257 Dicer in large cytoplasmic foci upon SINV and SFV infection in *M. myotis* nasal
258 epithelial cells that we did not witness in human cells (**Fig. 4** and **S2**). These Dicer foci
259 are in close proximity with dsRNA and SINV plus strand RNA, suggesting that Dicer is
260 recruited to sites of SINV replication (**Fig. 5**). Finally, mmDicer does not form these
261 foci when expressed in human Dicer knock out cells, suggesting that its relocalization
262 requires specific factors that are present in *M. myotis* nasal epithelial cells (**Fig. 6**).
263 Our results that mmDicer does not have increased antiviral RNAi activity is
264 unexpected in view of the recently published results on *P. alecto* and *T. brasiliensis*
265 Dicer, especially as SINV was also used in the *P. alecto* study (Dai *et al*, 2024; Owolabi
266 *et al*, 2025). This discrepancy could come from differences in bat species, as *P. alecto*
267 and *M. myotis* are thought to have diverged more than 60 million years ago, and *T.*
268 *brasiliensis* and *M. myotis* at least 35 million years ago (Teeling *et al*, 2005; Agnarsson
269 *et al*, 2011; Hao *et al*, 2024). Since in human and mouse cells the antiviral RNAi activity
270 of Dicer can be cell-type dependent, it is also possible that the activity of bat Dicer is
271 influenced by the cell type used in each study, especially if different bat species and
272 cell types have differences in IFN activity (Geng *et al*, 2024; Bondet *et al*, 2021;
273 Clayton & Munir, 2020). In mammalian cells, the same Dicer protein could play a role
274 in antiviral immunity through its RNAi activity, but also through direct regulation of the
275 innate immune reponse and through the maturation of miRNAs that regulate the innate
276 immune response (Gaucherand *et al*, 2024; Maillard *et al*, 2019). These multiple
277 interconnected activities of Dicer make the study of Dicer antiviral activity difficult. We
278 employed a transient siRNA knockdown strategy instead of knocking out Dicer to limit
279 the impact of removing Dicer on the expression of miRNAs, which have a notoriously
280 long half-life (Marzi *et al*, 2016), but there could still be indirect effects of Dicer
281 influencing its propensity to be anti- or proviral in specific cellular contexts. In general,
282 it will be important to study the activity of Dicer in more bat species to resolve this
283 discrepancy.
284 The case of VSV is interesting, as knocking down Dicer in *M. myotis* cells led to
285 an increase in VSV-GFP RNA and proteins levels (**Fig. 2F-G**). Yet, there was almost
286 no viral siRNAs (**Fig. 3, Fig S1**). The mechanism behind this apparent antiviral activity
287 of Dicer is thus unclear. Nonetheless, it serves as a good control of a virus that does
288 not trigger relocalization of Dicer in *M. myotis* cells, suggesting that this relocalization

289 is context-specific and not an artefact of infection. Since dsRNA is not detectable upon
290 VSV infection unlike infection with alphaviruses, it is tempting to hypothesize that the
291 relocalization of Dicer is linked to dsRNA accessibility. It will be interesting to test this
292 hypothesis.

293 Dicer relocalization to discreet cytoplasmic foci upon infection in *M. myotis* cells is
294 reminiscent of *Drosophila* D2 bodies (Nishida *et al*, 2013). These D2 bodies are
295 cytoplasmic foci containing Dicer-2 and its co-factor R2D2 that are important for the
296 processing of endogenous siRNAs in *Drosophila* cells. Yet, our small RNAseq results
297 did not identify such activity of Dicer. Moreover, we see a proviral effect instead of an
298 antiviral effect associated with Dicer relocalization, although it remains purely
299 correlative as we do not have concrete evidence so far that the two are directly linked.
300 We can nonetheless propose several hypotheses as to how the relocalization of Dicer
301 could play a proviral role. Potential consequences of this relocalization could be the
302 sequestration of Dicer by SINV, for example to prevent Dicer activity as part of the
303 antiviral RNAi pathway. Alternatively, Dicer could be recruited to sites of SINV
304 replication to hide dsRNA from PRRs or to directly tone down the local innate immune
305 response. One possible explanation for this recruitment, which remains to be tested,
306 could be that mmDicer has a higher affinity for dsRNA than its human counterpart in
307 *M. myotis* cells, maybe thanks to specific co-factors, but with no increased cleavage
308 activity. Dicer could also have a structural role to help viral factory formation and
309 alphavirus replication. More work will be needed to identify the purpose of Dicer
310 relocalization and the link between this relocalization and Dicer proviral activity.

311 It is intriguing that this relocalization does not appear to occur in human cells, or
312 at least in the human cell lines that we have tested. The fact that mmDicer alone is not
313 sufficient for relocalization is consistent with mmDicer and hDicer being very similar,
314 with 95% conservation between the two proteins at the amino acid level. Work to
315 identify the *M. myotis* cell specific factors responsible for Dicer relocalization is
316 ongoing. Host proteins that only interact with viral proteins in bat cells are good
317 candidates. On top of finding the mechanism of Dicer relocalization, it will also be
318 important to determine whether Dicer forms cytoplasmic foci during infection with other
319 viruses and in other stress conditions. It will especially be important to test viral strains
320 that are more biologically relevant to *M. myotis*. While many different alphaviruses
321 have been detected in several species of bats in the wild, including SINV and SFV, it
322 is still not clear whether bats constitute a reservoir for alphaviruses as this has not

323 been well studied (Fagre & Kading, 2019). Finally, it would be interesting to determine
324 if Dicer relocalization occurs in other bat species and cell types, and whether this
325 relocalization could explain the discrepancy in the observed antiviral RNAi activity of
326 Dicer.
327
328 **Materials and methods**
329 Cell culture and viral infections
330 SV40 transformed *M. myotis* nasal epithelial cells (He *et al*, 2014b) were a kind gift
331 from Bernd Köllner (FLI, Greifswald, Germany) through Lucie Etienne (CIRI, Lyon,
332 France). HEK293T/NoDice (2.20) cells (Bogerd *et al*, 2014) were a kind gift from Bryan
333 Cullen (Duke University, Durham NC, USA). All cells were maintened in Dulbecco's
334 modified Eagle medium (DMEM, Gibco, Life Technologies) supplemented with 10%
335 fetal bovine serum (FBS, bioSera FB1090/500, Batch# S00O0) in a humidified
336 atmosphere of 5% CO_2 at 37°C.
337 WT SINV (strain AR339) and SINV-GFP (kindly provided by M. C. Saleh, Institut
338 Pasteur, Paris, France, Saleh et al., 2009) viral stocks were produced and amplified
339 in BHK21 cells. SFV (strain UVE/SFV/UNK/XX1745; EVAg 001V-02468) was
340 propagated in Vero E6 cells from the initial stock. WT VSV (strain Indiana isolate PI10)
341 and VSV-GFP (Mueller *et al*, 2010) were propagated in BHK21 cells from the initial
342 stock. Stock titrations were performed by plaque assay on VERO E6 cells. Cells were
343 infected at MOIs ranging from 0.02 to 20, for 8h or 24h, as indicated in the figure
344 legends.
345
346 Plasmids and cloning
347 pLenti6 Flag-HA-V5 vector was modified from pLenti6-V5 gateway vector (Thermo
348 Fisher scientific V49610) by Gibson cloning (New England Biolabs) as previously
349 described (Baldaccini *et al*, 2024), then further modified to remove the V5 tag and
350 ccdB cassette. plenti6 Flag-HA hDicer was already described (Baldaccini *et al*, 2024).
351 mmDicer was cloned from *M. myotis* nasal epithelial cells mRNA using Superscript IV
352 one-step RT-PCR (Thermo Fisher Scientific) with primers Forward
353 (CAGTGTGGTGGAATTCTGCAGAAAA GCCCTGCTTTGCAACCC) and Reverse
354 (CCAAACTCATTACTAACCGGTTCAGCTGCT GGGAACCTGAG). plenti6 Flag-HA-
355 V5 was digested with AgeI and PstI restriction enzymes, then ligated with amplified
356 mmDicer with matching overhangs by Gibson cloning (New England Biolabs).

357 Catalytic mutations (E1562A and E1819A) were introduced by PCR inside primers
358 Forward (GACTGCGTGGCTGCCCTGCTGGGCTGC TATTTAA) + Reverse
359 (AGCAGGGCAGCCACGCAGTCGGCGATGCTTTTGT) and Forward
360 (GGGATATTTTTGCTTCACTTGCTGGTGCCATTTAC) + Reverse (GCAAGTGA
361 AGCAAAAATATCCCCCATGGCCTTG), then ligated to AgeI and PstI digested plenti6
362 Flag-HA-V5 by Gibson cloning (New England Biolabs).
363
364 Lentivirus production and generation of stable cell lines
365 HEK23T cells were plated in 6 well plates and transfected with 0.33 µg pVSV envelope
366 plasmid (Addgene #8454) and 1.33 µg pSPAX2 packaging plasmid (Addgene
367 #12260), and 1.7 µg of either plenti6 Flag-HA Empty, plenti6 Flag-HA hDicer, plenti6
368 Flag-HA mmDicer or plenti6 Flag-HA mmDicer CM, using Lipofectamine 2000 reagent
369 (Invitrogen, Fisher Scientific) according to the manufacturer's protocol. Media was
370 replaced 6h later, then the supernatent containing viral particles was collected at 48h
371 and filtered through a 0.45 µm PES filter. HEK293T NoDice (Bogerd *et al*, 2014) were
372 then transduced with the filtered lentiviruses mixed with 4µg/ml polybrene. Efficiently
373 transduced cells were selected for several days with blasticidine at 15 µg/mL and
374 polyclonal populations were used for experiments.
375
376 Dicer knock down
377 *M. myotis* Dicer specific siRNAs were designed by siTOOLs Biotech to form a siPOOL
378 of 30 siRNAs. A siPOOL of 30 non-targeting siRNAs was used as control (siTOOLs
379 Biotech). *M. myotis* nasal epithelial cells were reverse transfected with siNeg or siDicer
380 at 3nM final siRNA concentration using Lipofectamine RNAiMax (ThermoFisher)
381 following siTOOLs Biotech instructions. Cells were transfected again the following day
382 with siNeg or siDicer at 3nM final siRNA concentration. The next day, cells were
383 collected to check for efficient knock down or infected with different viruses.
384
385 Live cell imaging
386 *M. myotis* nasal epithelial cells were treated with two rounds of siRNAs then infected
387 with SINV-GFP at MOI 0.2. Cells were then placed into a CellCyte X live cell imaging
388 system (Cytena) where GFP fluorescence and phase contrast pictures (10X objective)
389 of every well were taken every 3h for 72h. The percentage of GFP+ area over the total

390 cell area was quantified with the CellCyte Studio software and averaged from six
391 photos of 2 individual wells per condition.
392
393 Protein extraction and western blot
394 Proteins were harvested and homogenized in appropriate quantity of ice cold lysis
395 buffer (50 mM Tris-HCl pH 7.5, 150 mM NaCl, 5 mM EDTA, 1% Triton X-100, 0.5%
396 SDS protease free inhibitor tablet (complete Mini; Sigma Aldrich)). Protein amounts
397 were quantified using Bradford reagent (Bio-Rad), diluted in lysis buffer + Laemmli and
398 boiled for 5 min before loading. Proteins were loaded on 10% acrylamide-bis-
399 acrylamide gels, or 4–20% Mini-PROTEAN TGX Precast Gels (Bio-Rad) for the Dicer
400 immunoprecipitation experiment. Proteins were separated by migration at 140 V in 1X
401 Tris-Glycine-SDS buffer (Euromedex), then electro-transferred on a nitrocellulose
402 membrane (Amersham 0.45 µm) in 1X Tris-Glycine buffer supplemented with 10%
403 ethanol. Appropriate loading and transfer efficiency were verified by Ponceau S
404 staining (Merck). Membranes were blocked in 5% milk diluted in PBS-Tween 0.2%.
405 Membranes were stained with primary antibodies overnight at 4 °C at the following
406 dilutions: anti-DICER (1:2000, A301-937A, Euromedex, Bethyl), anti-HA-HRP
407 (1:1000, 12013819001 Merck, Sigma Aldrich), anti-GFP (1:1000, 11814460001
408 Merck, Sigma Aldrich), anti-SINV nsp2 (1:5000, kind gift from Diane Griffin, Johns
409 Hopkins University School of Medicine, Baltimore, MD), anti-PKR (1:1000, ab32506
410 Abcam), anti-PACT (1:500, ab75749 Abcam), anti-TRBP (1:500, sc-514124,
411 Cliniscience, Santa Cruz), anti-ADAR1 (1:1000, E6X9R #81284 Cell Signaling), anti-
412 α-Tubulin-HRP (1:10000, Sigma, T6557). After several washes with PBS-Tween 0.2%,
413 the membranes were stained with the following secondary antibodies coupled to
414 horseradish peroxidase (HRP): anti-mouse-HRP (1:4000, A4416 Merck, Sigma-
415 Aldrich) or anti-rabbit-HRP (1:10,000, NA9340V Cytiva, Sigma-Aldrich). Detection was
416 carried out using SuperSignal West Femto maximum sensitivity substrate (Pierce,
417 Fisher Scientific) and visualized with a Fusion FX imaging system (Vilber).
418
419 Plaque assay
420 For SINV-GFP infections, Vero E6 cells were seeded in 96-well plates and infected
421 with 10-fold serial dilutions of infection supernatants. After 1 hour, the inoculum was
422 removed and cells were covered with 2.5% carboxymethyl cellulose and cultured for
423 72 hours at 37°C in a humidified atmosphere of 5% CO2. Plaques were counted

424 manually under the microscope. For SFV and VSV-GFP infections, Vero E6 cells were
425 seeded in 12-well plates and infected with 10-fold serial dilutions of infection
426 supernatants. After 1 hour, the inoculum was removed, cells were covered with 1.2%
427 Avicel overlay (vivapur mcg, JRS Pharma) and cultured for 48 hours at 37°C in a
428 humidified atmosphere with 5% CO2. Cells were then washed and fixed with 4%
429 formaldehyde (Merck, Sigma Aldrich) in PBS (phosphate buffered saline, Gibco) for
430 20 minutes, then stained with crystal violet for 5 minutes (Sigma-Aldrich). Plates were
431 washed with water and plaques were counted manually. Viral titers were calculated
432 according to the formula: PFU/mL = #plaques/ (Dilution*Volume of inoculum).
433
434 RNA and small RNA extractions
435 Total RNA was extracted from cell lysates using Trizol Reagent (15586018, InVitrogen)
436 to which 200 µl of chloroform was added before centrifugation for 15 minutes at 12,000
437 xg at 4°C. For regular RNA extraction, the aqueous layer was collected and nucleic
438 acids were precipitated in an equal volume of isopropanol for 10 min at room
439 temperature. For small RNA extraction, the aqueous layer was collected and nucleic
440 acids were precipitated in 3 volumes of 100% ethanol + 10% 1M sodium acetate for
441 30 minutes at -80°C. In both cases, precipitated RNA was then pelleted for 10 min at
442 12,000 xg at 4°C then washed with 70% ethanol and reconstituted in RNase free
443 water.
444
445 Northern blot analysis
446 3 µg of total RNA was loaded onto a 17% urea acrylamide gel and electro separated
447 in a 1X Tris-Borate-EDTA solution. The RNA was then electro transferred to a Hybond-
448 NX membrane (GE Healthcare), and chemically cross linked to the membrane with 1-
449 ethyl-3-[3-dimethylaminopropyl]carbodiimide hydrochloride (EDC) (Sigma Aldrich) for
450 90 min at 65°C. Membranes were then pre-hybridized for 30 min with PerfectHyb plus
451 (Sigma Aldrich) at 50°C. Probes consisting of an oligodeoxyribonucleotide sequence
452 for which the 5′- was labelled with 25 µCi of [γ-32P]dATP using T4 polynucleotide
453 kinase (Thermo Fisher Scientific) were incubated overnight with the membranes at
454 50°C. The membranes were then washed twice at 50°C for 10 min with 5X SSC/0.1%
455 SDS, then for 5 min with 1X SSC/0.1% SDS. Finally, membranes were placed in
456 contact with a phosphorimager plate overnight and imaged with a Bioimager FLA-7000

457 scanner (Fuji). Probe sequences: miR-16 (CGCCAATATTTACGTGCTGCTA), U6
458 (GCAGGGGCCATGCTAATCTTCTCTGT ATCG).
459
460 RT-qPCR analysis
461 After RNA extraction, samples were incubated with DNase I (Invitrogen, Fisher
462 Scientific) for 20 min at 37°C. The RNA was then reverse-transcribed into cDNA using
463 SuperScript IV (SSIV) reverse transcriptase (Invitrogen, Fisher Scientific) or AMV
464 reverse transcriptase (Promega) with a random nonameric primer, following the
465 manufacturer's protocol. Quantitative real-time PCR was performed using SYBR
466 Green PCR Master Mix (Fisher Scientific) and the following primers: 18S F
467 (CTCTTAGCTGAGTGTCCCGC), 18S R (CTTAATCATGGCCTCAGTTCCGA), SINV
468 F (CCACTACGCAAGCAGAGACG), SINV R (AGTGCCCAGGGCCTGTGTCCG),
469 VSV F (TGTACAATCAGGCGAGAGTC), VSV R
470 (GGAACTCATGATGAATGGATTGGG).
471
472 Small RNA sequencing and bioinformatic analysis
473 After small RNA extraction, samples were ran on a Bioanalyzer chip to confirm RNA
474 integrity. Samples were then shipped to BGI for library preparation with unique
475 molecular identifiers, and sequenced as single-end 50 base reads on their DNBSEQ
476 sequencing technology platform with at least 20 million reads per sample.
477 Raw reads were pre-cleaned by the sequencing platform, including adapter,
478 contaminant and low-quality removal (Phred+33). Before alignment, redundant
479 sequences were collapsed to one copy using fastq_collapser from FASTX-Toolkit
480 0.0.14 (http://hannonlab.cshl.edu/fastx_toolkit/) and a read-size filter was applied (18-
481 35 bp). HEK293T and *M. myotis* short reads were then aligned to the human genome
482 assembly GRCh38 (GCF_000001405.40) and the *M. myotis* genome mMyoMyo1.p
483 (GCF_014108235.1), respectively. Mapping was performed using Bowtie 1.3.1
484 (Langmead *et al*, 2009) with parameters '-v 1 -a --best --strata'. Unmapped reads were
485 next separately aligned against virus genomes SINV-GFP (private sequence derived
486 from NC_001547.1 – RefSeq database) and VSV-GFP (FJ478454.1) using the
487 following parameters '-v 2 -y -q -m 30 -a --best --strata'. Finally, siRNA signature was
488 examined on 22nt mapped reads by the python tool signature by (Antoniewski, 2014)
489 with options '22 22 1 22'. Sequencing data have been deposited on NCBI's Gene

490 Expression Omnibus (Edgar *et al*, 2002) and are accessible through GEO Series
491 accession number GSE301457.
492
493 Immunostaining
494 Cells were seeded onto Labtek eight-chamber slides (Nunc Lab Tek Chamber Slide
495 System) at a density of 8,000 cells per well. The next day, cells were infected for 8h or
496 24h with WT SINV, WT VSV or SFV. Cells were then fixed for 10 minutes at room
497 temperature with 4% formaldehyde (Sigma-Aldrich) diluted in 1X PBS. Blocking was
498 carried out with 5% normal goat serum in 0.1% Triton X-100 in 1X PBS for 1 hour at
499 room temperature. Primary antibody staining was carried out for 3h at room
500 temperature using the following antibodies diluted in blocking buffer: anti-Dicer
501 (1:1000, A301-937A, polyclonal, Bethyl) and J2 anti-dsRNA (1:1000, RNT-SCI-
502 10010200, Jena Bioscience). The cells were then incubated for 1 hour at room
503 temperature with secondary antibodies goat anti-mouse Alexa 594 (A11032,
504 Invitrogen) or goat anti-rabbit Alexa 488 (A11008, Invitrogen), both diluted at 1:1000
505 in 1X PBS with 0.1% Triton X-100. Between each step, cells were washed thoroughly
506 with 1X PBS containing 0.1% Triton X-100. Nuclei were stained with DAPI (4',6-
507 diamidino-2-phenylindole, dichlorhydrate, D1306, Thermo Fisher) at 1:5000 in 1X PBS
508 for 5 minutes. Finally, the slides were mounted with coverslips using Fluoromount-G
509 mounting media (Southern Biotech) and observed under a confocal microscope
510 (LSM780, Zeiss).
511
512 Sequential immunostaining and FISH
513 Mock- or WT SINV-infected cells were cultured on 18 mm round coverslips placed in
514 12-well plates. Cells were fixed with 3,7% formaldehyde (Sigma-Aldrich) diluted in 1X
515 PBS for 10 minutes at room temperature. Following fixation, cells were permeabilized
516 with 0.1% Triton X-100 in 1X PBS for 5 minutes at room temperature. Immunostaining
517 was performed as described in the previous section but with 1h incubation steps for
518 primary and secondary antibody staining. Subsequently, cells were fixed again with
519 3.7% formaldehyde (Sigma-Aldrich) diluted in 1X PBS for 10 minutes at room
520 temperature. For RNA detection, cells were incubated overnight at room temperature
521 with SINV genome-specific Stellaris Cal Fluor Red 610 RNA FISH Probes (LGC
522 Biosearch Technologies, custom made by Erika Girardi (Messmer *et al*, 2024)), kindly
523 provided by Erika Girardi (IBMC, Strasbourg, France). Probes were diluted in RNA

524 FISH hybridization buffer (Stellaris, Biosearch Technologies). Nuclei were stained with
525 DAPI (D1306, Invitrogen, Thermo Fisher Scientific) for 30 minutes. Finally, coverslips
526 were mounted using Fluoromount-G mounting medium (Invitrogen, Thermo Fisher
527 Scientific), and the samples were imaged by fluorescence microscopy (Olympus
528 BX51).
529
530 Image analysis
531 All image analyses were performed on confocal images and using the Fiji software
532 (Schindelin *et al*, 2012). Detection thresholds and all parameters were standardized
533 between the different images and cell lines to ensure consistency in the analysis. Each
534 analysis was performed on two (SFV) or three (SINV) biological replicates, with each
535 field containing approximately the same number of cells. The “Plot profile” tool on Fiji
536 was used to visualize fluorescent intensity as a function of distance for each channel.
537 The selection of the line or field of observation was made arbitrarily to best represent
538 the whole slide. Threshold parameters were adjusted accordingly to measure the size
539 of various objects, and the minimum size accepted was set to 0.1 μm^2 to limit
540 background detection. The “Analyse particle” tool was used to extract numerical data,
541 which was then systematically analyzed. The colocalization analysis between two
542 fluorescent signals was performed using the "Colocalization Finder" tool in Fiji. This
543 tool analyzes colocalization on a pixel-by-pixel basis by comparing the intensity of
544 each pixel in one channel to the corresponding pixel in the second channel of a bi-
545 color image. Importantly, the thresholds or brightness levels in the image are not
546 changed during this process. The analysis generates a scatter plot, from which a
547 Pearson correlation coefficient is calculated. A value of +1 indicates perfect correlation,
548 0 indicates no correlation, and -1 signifies perfect anti-correlation.
549
550 Dicer immunoprecipitation
551 NoDice cells expressing different HA-tagged Dicer constructs were plated and mock-
552 infected or infected with SINV-GFP at MOI 0.02. 24 hours later, cells were harvested,
553 washed twice with ice-cold 1X PBS (Gibco, Life Technologies), and resuspended in
554 lysis buffer (50 mM Tris-HCl pH 7.5, 140 mM NaCl, 6 mM MgCl2, 0.1% NP-40),
555 supplemented with a Complete-EDTA-free Protease Inhibitor Cocktail tablet (complete
556 Mini; Sigma Aldrich). Cells were lysed on ice for 10 min and debris were removed by
557 10 min centrifugation at 12,000 *xg* at 4°C. An aliquot of the cleared lysates was kept

558 aside as protein input. The rest of the samples were divided in two equal volumes and
559 incubated with 40 µL magnetic microparticles coated with monoclonal anti-HA or anti-
560 MYC antibodies (MACS purification system, Miltenyi Biotech) at 4°C for 1 hour with
561 constant rotation. Next, samples were passed through µ Columns (MACS purification
562 system, Miltenyi Biotech) and washed four times with 200 µL lysis buffer. Finally,
563 proteins were eluted with 2X Laemmli buffer (10% glycerol, 4% SDS, 62.5 mM TrisHCl
564 pH 6.8, 5% (v/v) 2-β-mercaptoethanol, Bromophenol Blue) that was pre-warmed to
565 95℃.
566

567 **Acknowledgements**

568 We would like to thank members of the laboratory for insightful discussions and
569 suggestions. This work of the Interdisciplinary Thematic Institute IMCbio+, as part of
570 the ITI 2021-2028 program of the University of Strasbourg, CNRS and Inserm, was
571 supported by IdEx Unistra (ANR-10-IDEX-0002), by SFRI-STRAT'US project (ANR-
572 20-SFRI-0012), EUR IMCBio (IMCBio ANR-17-EURE-0023) under the framework of
573 the French Investments for the Future Program. It was also supported by an Agence
574 Nationale pour la Recherche PRCI grant to SP (ANR-21-CE35-0018-01). LG was
575 funded by a postdoctoral fellowship from the Fondation pour la Recherche Médicale
576 (funding number SPF202209015746).
577

578 **References**

579 Agnarsson I, Zambrana-Torrelio CM, Flores-Saldana NP & May-Collado LJ (2011) A
580 time-calibrated species-level phylogeny of bats (Chiroptera, Mammalia). *PLoS*
581 *Currents* 3: RRN1212
582 Antoniewski C (2014) Computing siRNA and piRNA Overlap Signatures. In *Animal*
583 *Endo-SiRNAs: Methods and Protocols*, Werner A (ed) pp 135–146. New York, NY:
584 Springer
585 Baldaccini M, Gaucherand L, Chane-Woon-Ming B, Messmer M, Gucciardi F & Pfeffer
586 S (2024) The helicase domain of human Dicer prevents RNAi-independent
587 activation of antiviral and inflammatory pathways. *EMBO J* 43: 806–835
588 Baldaccini M & Pfeffer S (2021) Untangling the roles of RNA helicases in antiviral
589 innate immunity. *PLOS Pathogens* 17: e1010072
590 Banerjee A, Baker ML, Kulcsar K, Misra V, Plowright R & Mossman K (2020) Novel
591 Insights Into Immune Systems of Bats. *Frontiers in Immunology* 11

592 Bartel DP (2018) Metazoan MicroRNAs. *Cell* 173: 20–51
593 Bogerd HP, Whisnant AW, Kennedy EM, Flores O & Cullen BR (2014) Derivation and
594 characterization of Dicer- and microRNA-deficient human cells. *RNA* 20: 923–937
595 Bondet V, Le Baut M, Le Poder S, Lécu A, Petit T, Wedlarski R, Duffy D & Le Roux D
596 (2021) Constitutive IFNα Protein Production in Bats. *Front Immunol* 12: 735866
597 Burgin CJ, Colella JP, Kahn PL & Upham NS (2018) How many species of mammals
598 are there? *Journal of Mammalogy* 99: 1–14
599 Chua KB, Lek Koh C, Hooi PS, Wee KF, Khong JH, Chua BH, Chan YP, Lim ME &
600 Lam SK (2002) Isolation of Nipah virus from Malaysian Island flying-foxes.
601 *Microbes and Infection* 4: 145–151
602 Clayton E & Munir M (2020) Fundamental Characteristics of Bat Interferon Systems.
603 *Front Cell Infect Microbiol* 10: 527921
604 Cullen BR, Cherry S & tenOever BR (2013) Is RNA Interference a Physiologically
605 Relevant Innate Antiviral Immune Response in Mammals? *Cell Host & Microbe*
606 14: 374–378
607 Dai Y, Wang B, Wang J, Wei X, Liu X, Che X, Li J, Lun Ng W, Wang L-F & Li Y (2024)
608 Increased viral tolerance mediates by antiviral RNA interference in bat cells. *Cell*
609 *Reports* 43: 114581
610 Edgar R, Domrachev M & Lash AE (2002) Gene Expression Omnibus: NCBI gene
611 expression and hybridization array data repository. *Nucleic Acids Res* 30: 207–
612 210
613 Fagre AC & Kading RC (2019) Can Bats Serve as Reservoirs for Arboviruses? *Viruses*
614 11: 215
615 Flemr M, Malik R, Franke V, Nejepinska J, Sedlacek R, Vlahovicek K & Svoboda P
616 (2013) A retrotransposon-driven dicer isoform directs endogenous small
617 interfering RNA production in mouse oocytes. *Cell* 155: 807–816
618 Gaucherand L, Baldaccini M & Pfeffer S (2024) Beyond RNAi: How the Dicer protein
619 modulates the antiviral innate immune response in mammalian cells. *Bioessays*:
620 e2400173
621 Geng R, Wang Q, Yao Y-L, Shen X-R, Jia J-K, Wang X, Zhu Y, Li Q, Shi Z-L & Zhou P
622 (2024) Unconventional IFNω-like Genes Dominate the Type I IFN Locus and the
623 Constitutive Antiviral Responses in Bats. *The Journal of Immunology*: ji2300301

624 Girardi E, Chane-Woon-Ming B, Messmer M, Kaukinen P & Pfeffer S (2013)
625 Identification of RNase L-dependent, 3'-end-modified, viral small RNAs in Sindbis
626 virus-infected mammalian cells. *MBio* 4: e00698-00613
627 Gonzalez V & Banerjee A (2022) Molecular, ecological, and behavioral drivers of the
628 bat-virus relationship. *iScience* 25: 104779
629 Griffin D (2007) Alphaviruses, p 1023–1067. In *Fields virology, 5th ed. Lippincott*
630 *Williams & Wilkins, Philadelphia, PA*
631 Guo Z, Li Y & Ding S-W (2019) Small RNA-based antimicrobial immunity. *Nat Rev*
632 *Immunol* 19: 31–44
633 Gurung C, Fendereski M, Sapkota K, Guo J, Huang F & Guo Y-L (2021) Dicer
634 represses the interferon response and the double-stranded RNA-activated protein
635 kinase pathway in mouse embryonic stem cells. *Journal of Biological Chemistry*
636 296: 100264
637 Halpin K, Young PL, Field HE & Mackenzie JS (2000) Isolation of Hendra virus from
638 pteropid bats: a natural reservoir of Hendra virus. *Journal of General Virology* 81:
639 1927–1932
640 Hao X, Lu Q & Zhao H (2024) A molecular phylogeny for all 21 families within
641 Chiroptera (bats). *Integrative Zoology* 19: 989–998
642 He X, Korytář T, Schatz J, Freuling CM, Müller T & Köllner B (2014a) Anti-Lyssaviral
643 Activity of Interferons κ and ω from the Serotine Bat, Eptesicus serotinus. *Journal*
644 *of Virology* 88: 5444
645 He X, Korytář T, Zhu Y, Pikula J, Bandouchova H, Zukal J & Köllner B (2014b)
646 Establishment of Myotis myotis cell lines--model for investigation of host-pathogen
647 interaction in a natural host for emerging viruses. *PLoS One* 9: e109795
648 Irving AT, Ahn M, Goh G, Anderson DE & Wang L-F (2021) Lessons from the host
649 defences of bats, a unique viral reservoir. *Nature* 589: 363–370
650 Kulmann MIR, Taborska E, Benköova B, Palus M, Drobek A, Horvat F, Pasulka J, Malik
651 R, Salyova E, Hönig V, *et al* (2025) Enhanced RNAi does not provide efficient
652 innate antiviral immunity in mice. *Nucleic Acids Res* 53: gkae1288
653 Langmead B, Trapnell C, Pop M & Salzberg SL (2009) Ultrafast and memory-efficient
654 alignment of short DNA sequences to the human genome. *Genome Biol* 10: R25
655 Lee HY, Zhou K, Smith AM, Noland CL & Doudna JA (2013) Differential roles of human
656 Dicer-binding proteins TRBP and PACT in small RNA processing. *Nucleic Acids*
657 *Res* 41: 6568–6576

658 Lei M & Dong D (2016) Phylogenomic analyses of bat subordinal relationships based
659 on transcriptome data. *Sci Rep* 6: 27726
660 Li W, Shi Z, Yu M, Ren W, Smith C, Epstein JH, Wang H, Crameri G, Hu Z, Zhang H,
661 *et al* (2005) Bats Are Natural Reservoirs of SARS-Like Coronaviruses. *Science*
662 310: 676–679
663 López P, Girardi E, Mounce BC, Weiss A, Chane-Woon-Ming B, Messmer M, Kaukinen
664 P, Kopp A, Bortolamiol-Becet D, Fendri A, *et al* (2020) High-Throughput
665 Fluorescence-Based Screen Identifies the Neuronal MicroRNA miR-124 as a
666 Positive Regulator of Alphavirus Infection. *J Virol* 94
667 Maillard PV, Van der Veen AG, Deddouche-Grass S, Rogers NC, Merits A & Reis e
668 Sousa C (2016) Inactivation of the type I interferon pathway reveals long double-
669 stranded RNA-mediated RNA interference in mammalian cells. *EMBO J* 35: 2505–
670 2518
671 Maillard PV, van der Veen AG, Poirier EZ & Reis e Sousa C (2019) Slicing and dicing
672 viruses: antiviral RNA interference in mammals. *EMBO J* 38
673 Marzi MJ, Ghini F, Cerruti B, Pretis S de, Bonetti P, Giacomelli C, Gorski MG, Kress T,
674 Pelizzola M, Muller H, *et al* (2016) Degradation dynamics of microRNAs revealed
675 by a novel pulse-chase approach. *Genome Res*: gr.198788.115
676 Memish ZA, Mishra N, Olival KJ, Fagbo SF, Kapoor V, Epstein JH, AlHakeem R,
677 Durosinloun A, Al Asmari M, Islam A, *et al* (2013) Middle East Respiratory
678 Syndrome Coronavirus in Bats, Saudi Arabia. *Emerg Infect Dis* 19: 1819–1823
679 Messmer M, Pierson L, Pasquier C, Djordjevic N, Chicher J, Hammann P, Pfeffer S &
680 Girardi E (2024) DEAD box RNA helicase 5 is a new pro-viral host factor for
681 Sindbis virus infection. *Virol J* 21: 76
682 Montavon TC, Baldaccini M, Lefèvre M, Girardi E, Chane-Woon-Ming B, Messmer M,
683 Hammann P, Chicher J & Pfeffer S (2021) Human DICER helicase domain recruits
684 PKR and modulates its antiviral activity. *PLoS Pathog* 17: e1009549
685 Moratelli R & Calisher CH (2015) Bats and zoonotic viruses: can we confidently link
686 bats with emerging deadly viruses? *Mem Inst Oswaldo Cruz* 110: 1–22
687 Mueller S, Gausson V, Vodovar N, Deddouche S, Troxler L, Perot J, Pfeffer S,
688 Hoffmann JA, Saleh M-C & Imler J-L (2010) RNAi-mediated immunity provides
689 strong protection against the negative-strand RNA vesicular stomatitis virus in
690 Drosophila. *Proc Natl Acad Sci USA* 107: 19390–19395

691 Nishida KM, Miyoshi K, Ogino A, Miyoshi T, Siomi H & Siomi MC (2013) Roles of R2D2,
692 a cytoplasmic D2 body component, in the endogenous siRNA pathway in
693 Drosophila. *Mol Cell* 49: 680–691
694 Owolabi IJ, Karim S-U, Khanal S, Valdivia S, Frenzel C, Bai F & Flynt AS (2025)
695 Processing of genomic RNAs by Dicer in bat cells limits SARS-CoV-2 replication.
696 *Virology Journal* 22: 86
697 Pei G, Balkema-Buschmann A & Dorhoi A (2024) Disease tolerance as immune
698 defense strategy in bats: One size fits all? *PLOS Pathogens* 20: e1012471
699 Pichlmair A & Reis e Sousa C (2007) Innate recognition of viruses. *Immunity* 27: 370–
700 383
701 Poirier EZ, Buck MD, Chakravarty P, Carvalho J, Frederico B, Cardoso A, Healy L,
702 Ulferts R, Beale R & Reis e Sousa C (2021) An isoform of Dicer protects
703 mammalian stem cells against multiple RNA viruses. *Science* 373: 231–236
704 Richardson SJ, Willcox A, Hilton DA, Tauriainen S, Hyoty H, Bone AJ, Foulis AK &
705 Morgan NG (2010) Use of antisera directed against dsRNA to detect viral
706 infections in formalin-fixed paraffin-embedded tissue. *J Clin Virol* 49: 180–185
707 Schindelin J, Arganda-Carreras I, Frise E, Kaynig V, Longair M, Pietzsch T, Preibisch
708 S, Rueden C, Saalfeld S, Schmid B, *et al* (2012) Fiji: an open-source platform for
709 biological-image analysis. *Nat Methods* 9: 676–682
710 Teeling EC, Springer MS, Madsen O, Bates P, O'Brien SJ & Murphy WJ (2005) A
711 Molecular Phylogeny for Bats Illuminates Biogeography and the Fossil Record.
712 *Science* 307: 580–584
713 Towner JS, Pourrut X, Albariño CG, Nkogue CN, Bird BH, Grard G, Ksiazek TG,
714 Gonzalez J-P, Nichol ST & Leroy EM (2007) Marburg Virus Infection Detected in
715 a Common African Bat. *PLOS ONE* 2: e764
716 van der Veen AG, Maillard PV, Schmidt JM, Lee SA, Deddouche-Grass S, Borg A,
717 Kjær S, Snijders AP & Reis e Sousa C (2018) The RIG-I-like receptor LGP2 inhibits
718 Dicer-dependent processing of long double-stranded RNA and blocks RNA
719 interference in mammalian cells. *EMBO J* 37: e97479
720 Weber F, Wagner V, Rasmussen SB, Hartmann R & Paludan SR (2006) Double-
721 Stranded RNA Is Produced by Positive-Strand RNA Viruses and DNA Viruses but
722 Not in Detectable Amounts by Negative-Strand RNA Viruses. *J Virol* 80: 5059–
723 5064

724 Yob JM, Field H, Rashdi AM, Morrissy C, van der Heide B, Rota P, bin Adzhar A, White
725 J, Daniels P, Jamaluddin A, *et al* (2001) Nipah virus infection in bats (order
726 Chiroptera) in peninsular Malaysia. *Emerg Infect Dis* 7: 439–441
727

728 **Figure legends**

729 **Figure 1: Expressing *M. myotis* Dicer in human NoDice cells does not protect**
730 **from SINV and VSV infection. (A)** Expression of HA-tagged Dicer was analyzed by
731 western blot for NoDice cells expressing HA-tagged hDicer, mmDicer, mmDicer CM
732 or an empty vector control. α-Tubulin was used as loading control. Images are
733 representative of 3 independent experiments **(B)** Expression of miR-16 was analyzed
734 by northern blot for NoDice cells expressing HA-tagged hDicer, mmDicer, mmDicer
735 CM or an empty vector control. A probe for U6 snRNP was used as loading control.
736 Images are representative of 2 independent experiments. **(C-F)** NoDice cells
737 expressing HA-tagged hDicer, mmDicer, mmDicer CM or an empty vector control were
738 infected with SINV-GFP **(C-E)** or VSV-GFP **(F)** at MOI 0.02 for 24h. **(C, F)**
739 Supernatants were collected and viral titers were quantified by plaque assay. Means
740 +/- standard deviation are plotted for 4 **(C)** or 3 **(F)** independent experiments. **(D)**
741 Protein lysates were collected and analyzed by western blot using antibodies for SINV
742 nsp2 and GFP. α-Tubulin was used as loading control. n = 3 independent experiments.
743 Quantification of GFP or nsp2 band intensities relative to Tubulin band intensities were
744 quantified with ImageJ and the mean +/- standard deviation was plotted relative to
745 empty vector control for all three independent experiments. **(E)** RNAs were purified
746 and levels of SINV RNA were quantified by qRT-PCR. Means +/- standard deviation
747 normalized to 18S are plotted relative to empty vector control for 4 independent
748 experiments. For all graphs, p values were calculated using standard one-way ANOVA
749 with Dunnett's multiple comparison test. ns: not significant.

750

751 **Figure 2: Dicer is proviral for SINV and SFV in *M. myotis* nasal epithelial cells.**
752 **(A)** Expression of Dicer was analyzed by western blot in *M. myotis* nasal epithelial
753 cells after two rounds of siRNA targeting Dicer (siDicer) or a non-targeting control
754 (siNeg). α-Tubulin was used as loading control. Images are representative of 2
755 independent experiments. **(B-J)** *M. myotis* nasal epithelial cells treated with siRNAs
756 targeting Dicer (siDicer) or a non-targeting control (siNeg) were infected with SINV-
757 GFP for 24h at MOI 0.2 **(B-E)**, SFV for 24h at MOI 20 **(F-G)** or VSV-GFP for 8h at MOI
758 1 **(H-J)**. **(B)** The number of GFP+ cells as a proxy for infection were monitored over
759 time by live microscopy imaging. Percentages of GFP+ area were plotted for each
760 condition as the average of two wells, six photos per well, for one experiment. **(C, F,**
761 **H)** Supernatants were collected and viral titers were quantified by plaque assay.

762 Means +/- standard deviation are plotted for 3 independent experiments. **(D, I)** Protein
763 lysates were collected and analyzed by western blot using antibodies for GFP. α-
764 Tubulin was used as loading control. n = 3 independent experiments. Quantification of
765 GFP band intensities relative to Tubulin band intensities were quantified with ImageJ
766 and the mean +/- standard deviation was plotted relative to siNeg mock samples for
767 all three independent experiments. **(E, G, J)** RNAs were purified and levels of SINV
768 RNA **(E)**, SFV RNA **(G)** or VSV RNA **(J)** were quantified by qRT-PCR. Means +/-
769 standard deviation are plotted relative to siNeg infected samples for 3 independent
770 experiments. For all graphs, p values were calculated using unpaired t test. * $p<0.5$;
771 ns: not significant.
772
773 **Figure 3: No strong RNAi signature in *M. myotis* nasal epithelial cells.** HEK293T
774 or *M. myotis* nasal epithelial cells were mock infected or infected with SINV-GFP or
775 VSV-GFP, then small RNAs were extracted and sequenced. n = 2 independent
776 experiments, see figure S1 for data from other replicate. **(A)** Percent of total
777 sequencing reads that align to the human or *M. myotis* genome (black), the SINV-GFP
778 genome (blue) or the VSV-GFP genome (red) for each sample in HEK293T cells (left)
779 or *M. myotis* nasal epithelial cells (right). "rep" indicates the replicate number. **(B)**
780 Number of reads that align to SINV-GFP or VSV-GFP for each cell type based on the
781 read size. The total number of reads is further broken down into colors based on the
782 identity of the first nucleotide of the read: yellow for U, blue for A, purple for G and
783 black for C. **(C)** Location of the 22 nucleotide (nt) reads along the SINV-GFP or VSV-
784 GFP genome for each sample. The number of reads falling on the same nucleotide is
785 represented in red if the reads align to the genome (+ strand) and in blue if they align
786 to the anti-genome (- strand). **(D)** For each sample, 22 nt small RNA pairs that overlap
787 on + and - strands were analyzed and associated z-scores (Antoniewski, 2014) were
788 plotted for the indicated nucleotide overlaps.
789
790 **Figure 4: Dicer relocalizes to distinct cytoplasmic puncta upon infection in *M.*
791 *myotis* nasal epithelial cells. (A-C)** HEK293T were mock infected or infected with
792 WT SINV for 8h at MOI 0.2 **(A)** or 24h at MOI 0.02 **(B)**. *M. myotis* nasal epithelial cells
793 were mock infected or infected with WT SINV for 8h at MOI 5 **(A)** or 24h at MOI 2 **(B)**.
794 Localization of Dicer (yellow) was imaged by immunofluorescence and confocal
795 microscopy. DAPI staining (blue) indicates cell nuclei. Images are representative of at

796 least 3 independent experiments. Scale bars 10µm. **(C)** For each condition, the
797 number and size of Dicer foci in SINV infected *M. myotis* nasal epithelial cells were
798 plotted for 3 or 4 independent experiments with each 1 or 2 fields containing
799 approximately the same number of cells. The black horizontal bars represent the
800 median. The p value was calculated using an unpaired t test.
801
802 **Figure 5: Dicer likely relocalizes to SINV viral factories in *M. myotis* nasal**
803 **epithelial cells. (A-B)** HEK293T were mock infected or infected with WT SINV or SFV
804 for 24h at MOI 0.02. *M. myotis* nasal epithelial cells were mock infected or infected
805 with WT SINV or SFV for 24h at MOI 2 or 5 respectively. Localization of Dicer (yellow)
806 and dsRNA via J2 antibodies (magenta) was imaged by immunofluorescence and
807 confocal microscopy. DAPI staining (blue) indicates cell nuclei. Images are
808 representative of 3 (SINV) or 2 (SFV) independent experiments. Scale bars 10µm. Co-
809 localization between Dicer and dsRNA signals was quantified and Pearson correlation
810 R coefficients were calculated and plotted for 3 (SINV) or 2 (SFV) independent
811 experiments – mean (numerical value indicated in gray font above each bar) +/-
812 standard deviation **(B)**. A zoomed-in image of the boxed area in some merge images
813 was added. The graphs show the signals for each channel along the line drawn in the
814 zoomed in images. **(C)** HEK293T or *M. myotis* nasal epithelial cells were mock infected
815 or infected with WT SINV for 24h at MOI 0.02 or 4, respectively. Localization of Dicer
816 (yellow) by immunofluorescence and of SINV plus strand (+) RNA (magenta) by FISH
817 was imaged with a fluorescent microscope. DAPI staining (blue) indicates cell nuclei.
818 Images are representative of 2 independent experiments. Scale bars 10µm.
819
820 **Figure 6: *M. myotis* Dicer alone is not sufficient for relocalization.** HEK293T
821 NoDice cells expressing HA-tagged hDicer or mmDicer were mock infected or infected
822 with SINV-GFP for 24h at MOI 0.02. **(A)** Cells were then lysed, a small aliquot was
823 kept as input, and Dicer was immunoprecipitated with anti-HA coated magnetic beads
824 (IP Dicer) or anti-myc coated beads (IP ctrl). Eluted proteins were analyzed by western
825 blot using antibodies for the known hDicer interactors ADAR1, PKR, TRBP and PACT.
826 Anti-HA antibodies show efficient immunoprecipitation of hDicer and mmDicer. Images
827 representative of 2 independent experiments. **(B)** Localization of Dicer (yellow) and
828 dsRNA via J2 antibodies (magenta) was imaged by immunofluorescence and confocal

829 microscopy. DAPI staining (blue) indicates cell nuclei. Images are representative of 2
830 independent experiments. Scale bars 10μm.
831
832 **Figure S1: Small RNAseq results for the rest of HEK293T and *M. myotis* nasal**
833 **epithelial samples.** HEK293T or *M. myotis* nasal epithelial cells were mock infected
834 or infected with SINV-GFP or VSV-GFP, then small RNAs were extracted and
835 sequenced. n = 2 independent experiments, see figure 3 for data from other replicate.
836 **(A)** Number of reads that align to SINV-GFP or VSV-GFP for each cell type based on
837 the read size. The total number of reads is further broken down into colors based on
838 the identity of the first nucleotide of the read: yellow for U, blue for A, purple for G and
839 black for C. **(B)** Location of the 22 nucleotide (nt) reads along the SINV-GFP or VSV-
840 GFP genome for each sample. The number of reads falling on the same nucleotide is
841 represented in red if the reads align to the genome (+ strand) and in blue if they align
842 to the anti-genome (- strand). **(C)** For each sample, 22 nt small RNA pairs that overlap
843 on + and - strands were analyzed and associated z-scores (Antoniewski, 2014) were
844 plotted for the indicated nucleotide overlaps.
845
846 **Figure S2: No Dicer foci are found in other human cell lines and in VSV infected**
847 **cells. (A)** Human A549 and Huh7 cells were mock infected or infected with WT SINV
848 at 24h at MOI 0.2 and 0.02, respectively. Localization of Dicer (yellow) and dsRNA via
849 J2 antibodies (magenta) were imaged by immunofluorescence and confocal
850 microscopy. DAPI staining (blue) indicates cell nuclei. Images are representative of 2
851 independent experiments. Scale bars 10μm. **(B)** HEK293T or *M. myotis* nasal
852 epithelial cells were infected with WT VSV for 8h at MOI 1. Localization of Dicer
853 (yellow) and dsRNA via J2 antibodies (magenta) were imaged by immunofluorescence
854 and confocal microscopy. DAPI staining (blue) indicates cell nuclei. Images are
855 representative of 2 independent experiments.

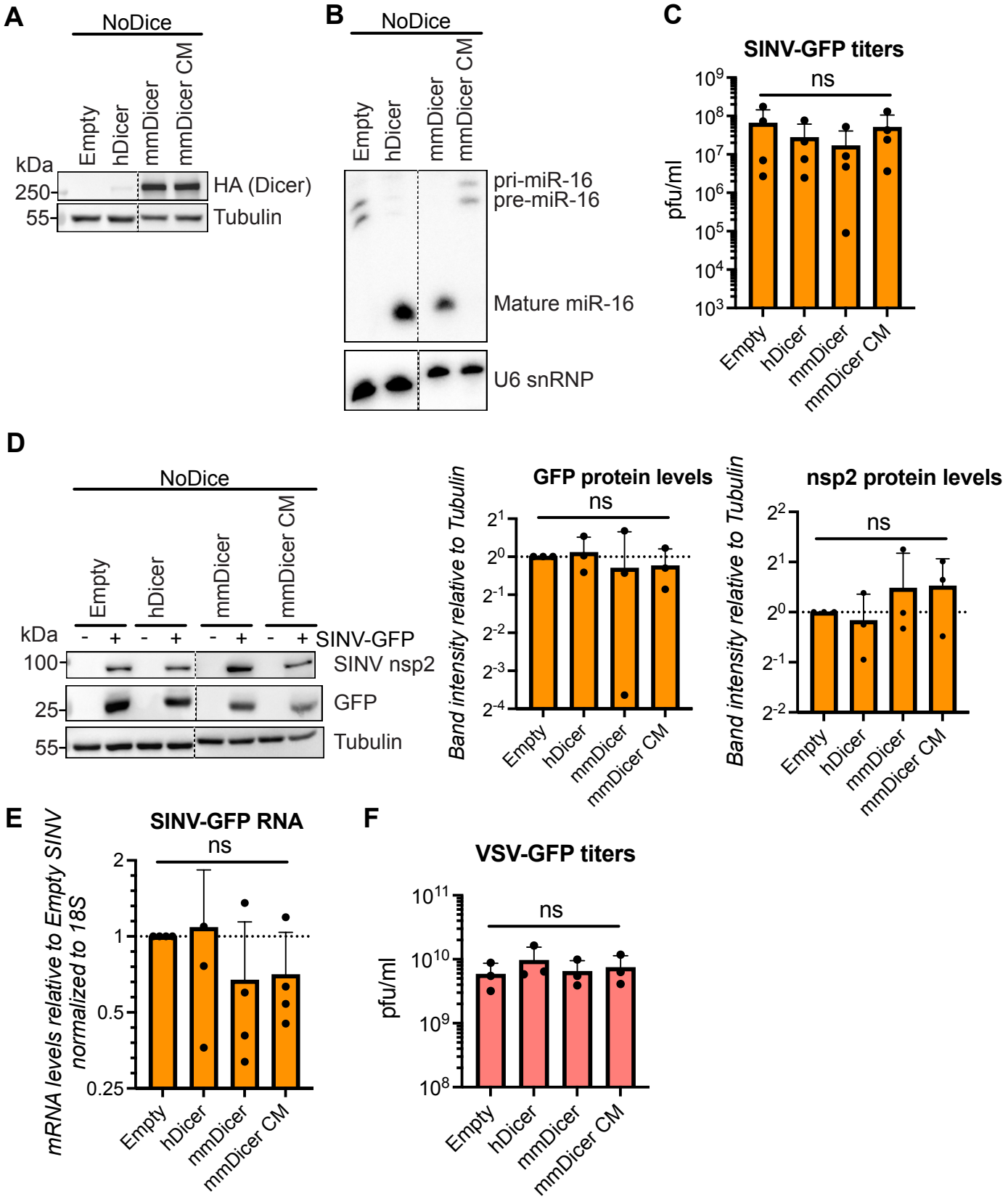
A
NoDice
Empty
hDicer
mmDicer
mmDicer CM
kDa
250
55
HA (Dicer)
Tubulin
B
NoDice
Empty
hDicer
mmDicer
mmDicer CM
pri-miR-16
pre-miR-16
Mature miR-16
U6 snRNP
C
SINV-GFP titers
ns
pfu/ml
Empty
hDicer
mmDicer
mmDicer CM
D
NoDice
Empty
hDicer
mmDicer
mmDicer CM
kDa
SINV-GFP
100
SINV nsp2
25
GFP
55
Tubulin
GFP protein levels
ns
Band intensity relative to Tubulin
nsp2 protein levels
ns
Band intensity relative to Tubulin
E
SINV-GFP RNA
ns
mRNA levels relative to Empty SINV normalized to 18S
F
VSV-GFP titers
ns
pfu/ml

Figure 1

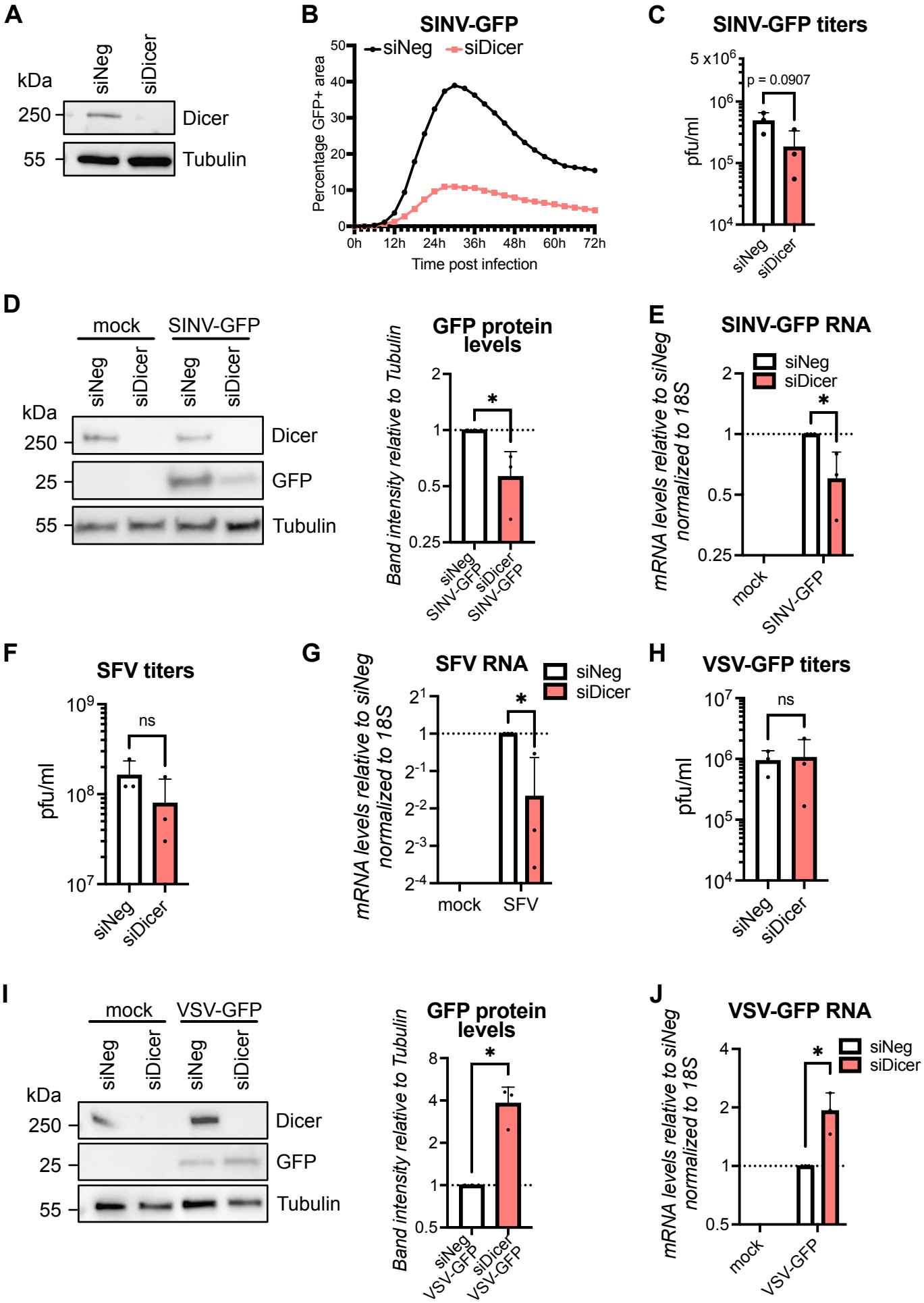
A
kDa
siNeg
siDicer
250
Dicer
55
Tubulin
B
SINV-GFP
siNeg
siDicer
Percentage GFP+ area
Time post infection
0h
12h
24h
36h
48h
60h
72h
C
SINV-GFP titers
p = 0.0907
pfu/ml
siNeg
siDicer
D
mock
SINV-GFP
kDa
250
25
55
Dicer
GFP
Tubulin
GFP protein levels
Band intensity relative to Tubulin
siNeg
SINV-GFP
siDicer
SINV-GFP
E
SINV-GFP RNA
mRNA levels relative to siNeg normalized to 18S
mock
SINV-GFP
F
SFV titers
ns
pfu/ml
G
SFV RNA
mRNA levels relative to siNeg normalized to 18S
mock
SFV
H
VSV-GFP titers
ns
pfu/ml
I
mock
VSV-GFP
kDa
250
25
55
Dicer
GFP
Tubulin
GFP protein levels
Band intensity relative to Tubulin
siNeg
VSV-GFP
siDicer
VSV-GFP
J
VSV-GFP RNA
mRNA levels relative to siNeg normalized to 18S
mock
VSV-GFP

Figure 2

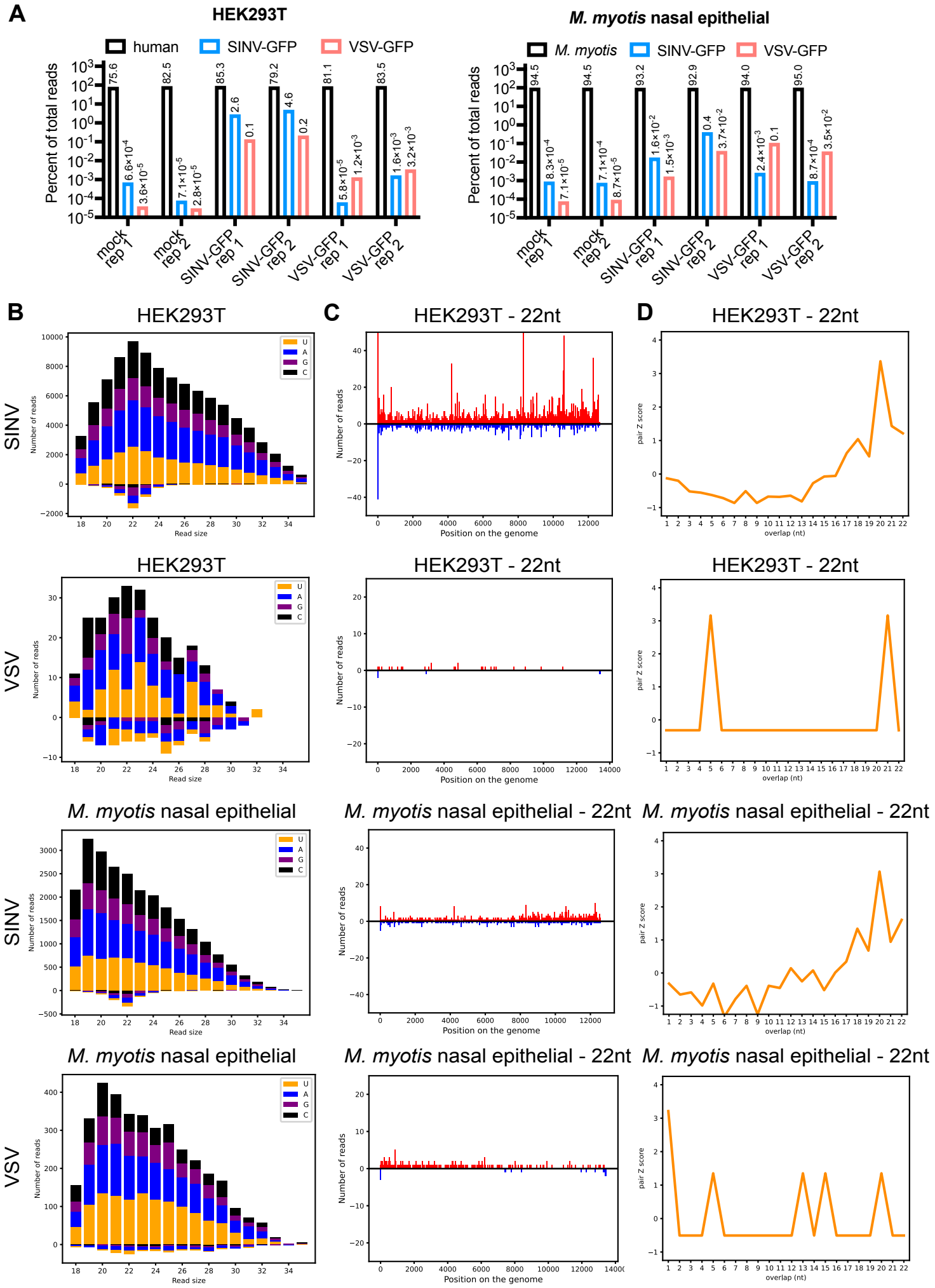
A
HEK293T
human
SINV-GFP
VSV-GFP
Percent of total reads
mock rep 1
mock rep 2
SINV-GFP rep 1
SINV-GFP rep 2
VSV-GFP rep 1
VSV-GFP rep 2
M. myotis nasal epithelial
M. myotis
B
C
D
SINV
VSV
Number of reads
Read size
Position on the genome
pair Z score
overlap (nt)
U
A
G
C

Figure 3

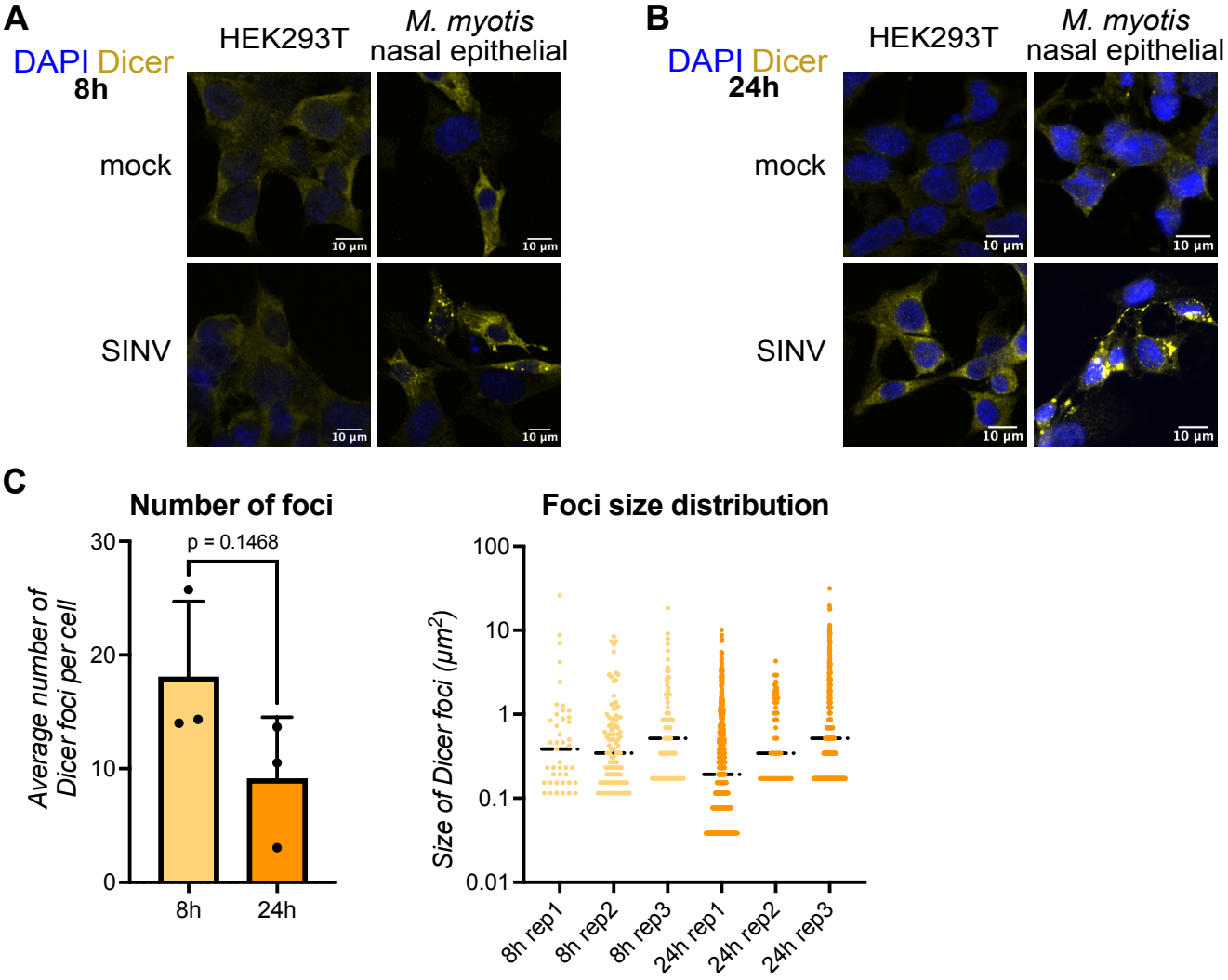
A
DAPI Dicer
8h
HEK293T
M. myotis
nasal epithelial
mock
SINV
10 µm
B
DAPI Dicer
24h
HEK293T
M. myotis
nasal epithelial
mock
SINV
10 µm
C
Number of foci
p = 0.1468
Average number of Dicer foci per cell
30
20
10
0
8h
24h
Foci size distribution
Size of Dicer foci (µm²)
100
10
1
0.1
0.01
8h rep1
8h rep2
8h rep3
24h rep1
24h rep2
24h rep3

Figure 4

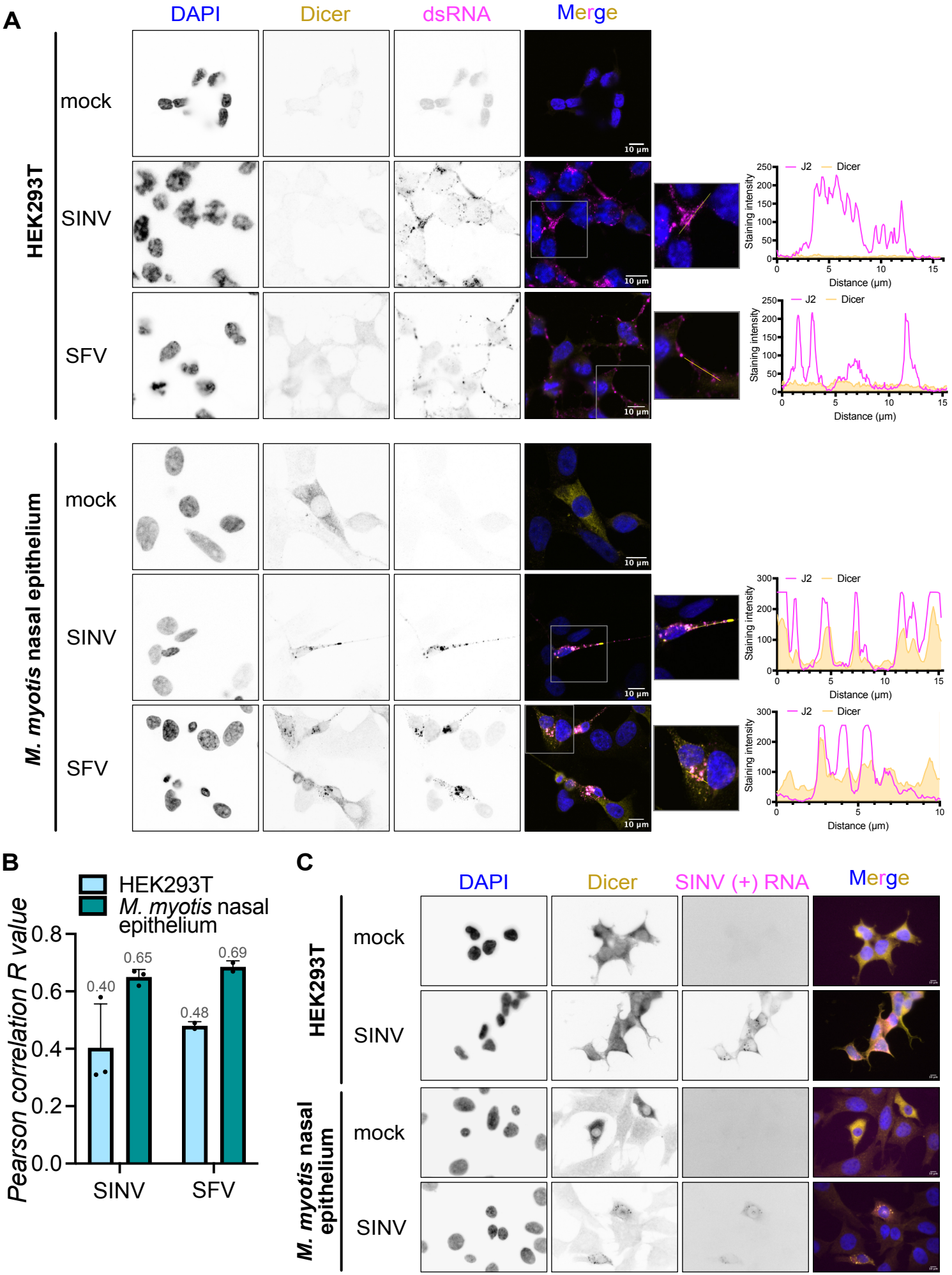
A
DAPI
Dicer
dsRNA
Merge
HEK293T
mock
SINV
SFV
10 µm
J2
Dicer
Staining intensity
Distance (µm)
M. myotis nasal epithelium
mock
SINV
SFV
B
HEK293T
M. myotis nasal epithelium
Pearson correlation R value
0.0
0.2
0.4
0.6
0.8
0.40
0.65
0.48
0.69
SINV
SFV
C
DAPI
Dicer
SINV (+) RNA
Merge
HEK293T
mock
SINV
M. myotis nasal epithelium
mock
SINV

Figure 5

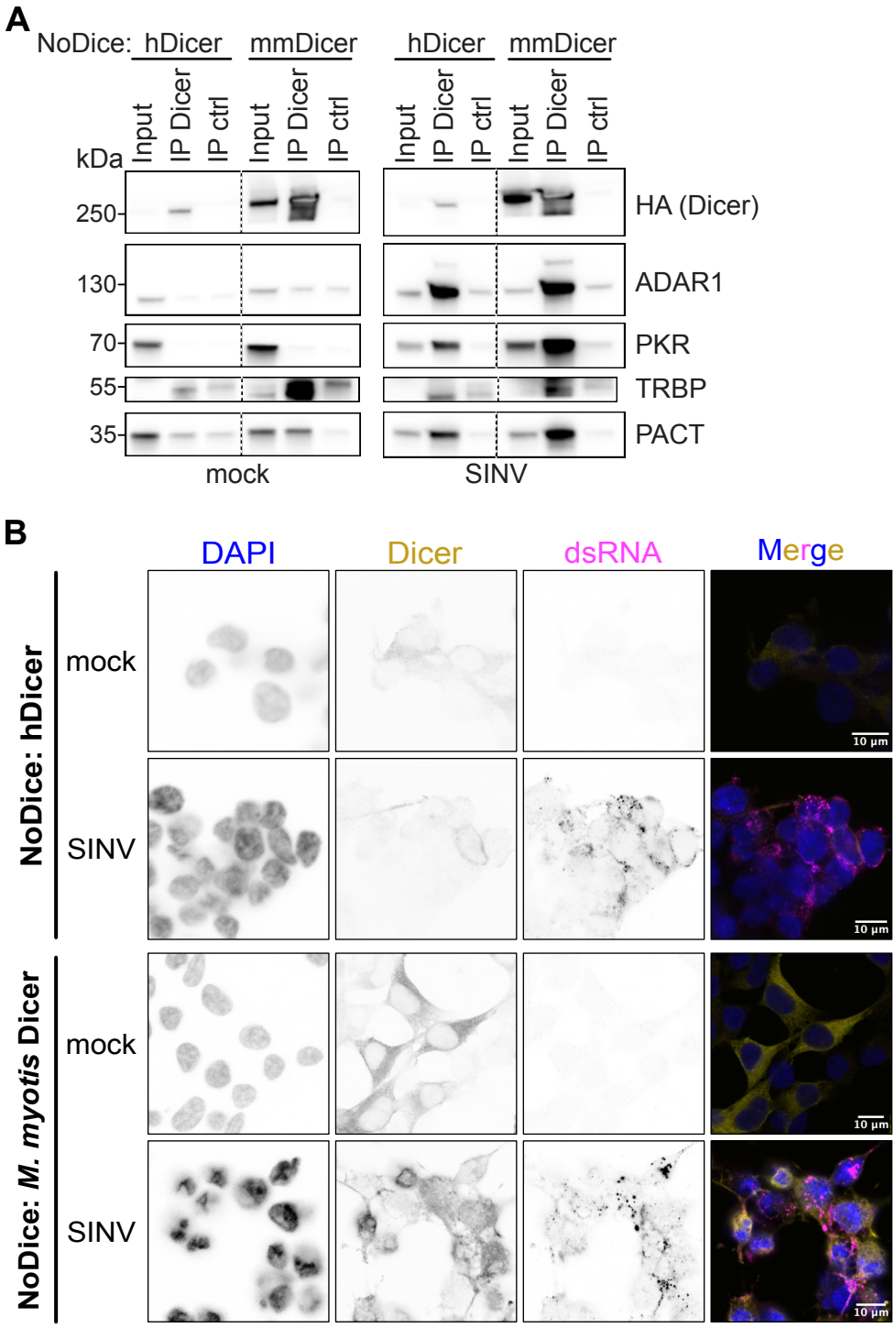
A
NoDice: hDicer mmDicer hDicer mmDicer
Input IP Dicer IP ctrl Input IP Dicer IP ctrl Input IP Dicer IP ctrl Input IP Dicer IP ctrl
kDa
250-
130-
70-
55-
35-
HA (Dicer)
ADAR1
PKR
TRBP
PACT
mock
SINV
B
DAPI
Dicer
dsRNA
Merge
NoDice: hDicer
mock
SINV
NoDice: M. myotis Dicer
mock
SINV
10 µm

Figure 6

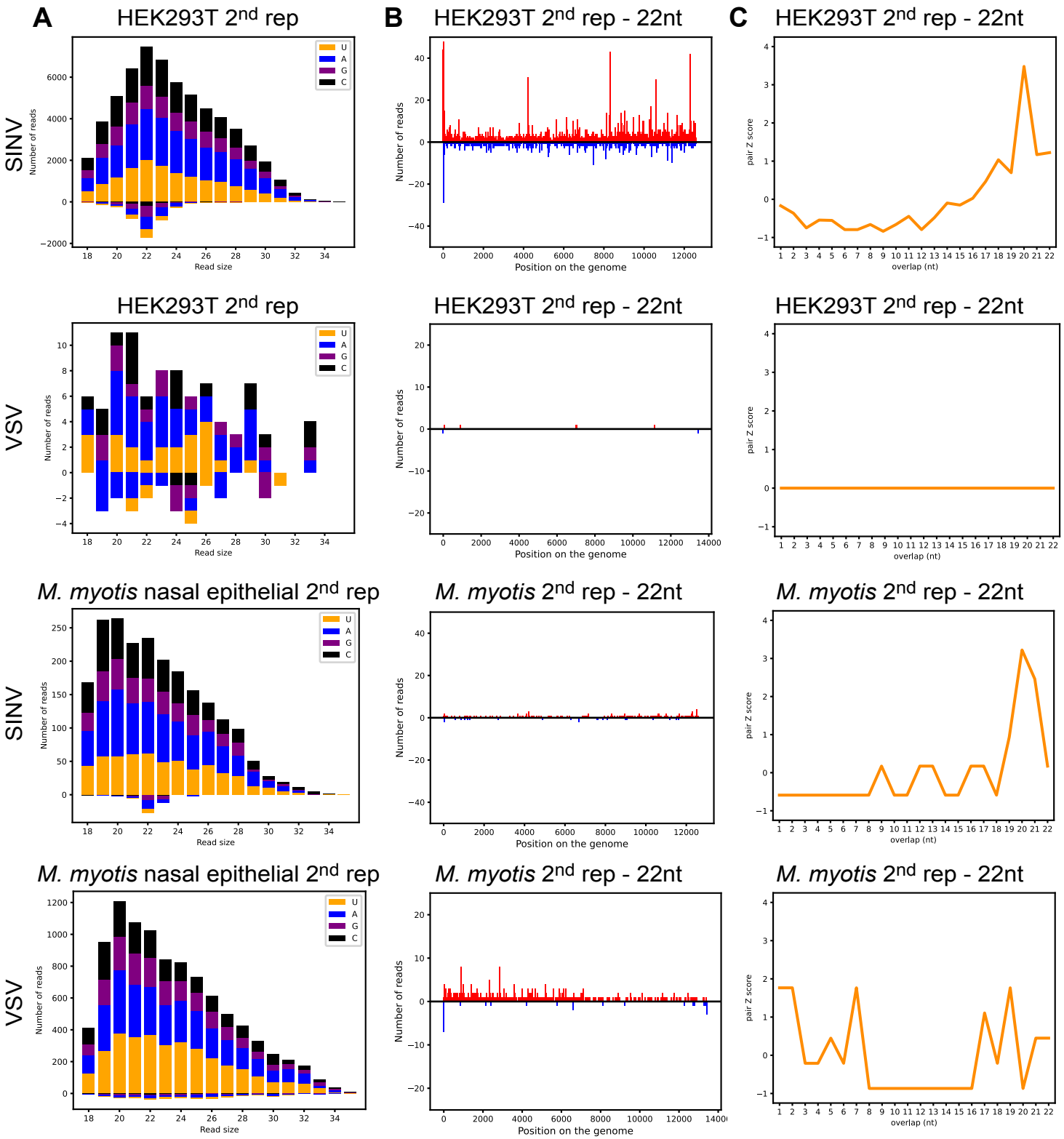
A
B
C
HEK293T 2nd rep
HEK293T 2nd rep - 22nt
HEK293T 2nd rep - 22nt
M. myotis nasal epithelial 2nd rep
M. myotis 2nd rep - 22nt
M. myotis 2nd rep - 22nt
SINV
VSV
SINV
VSV
U
A
G
C
Number of reads
Read size
Position on the genome
pair Z score
overlap (nt)

Figure S1

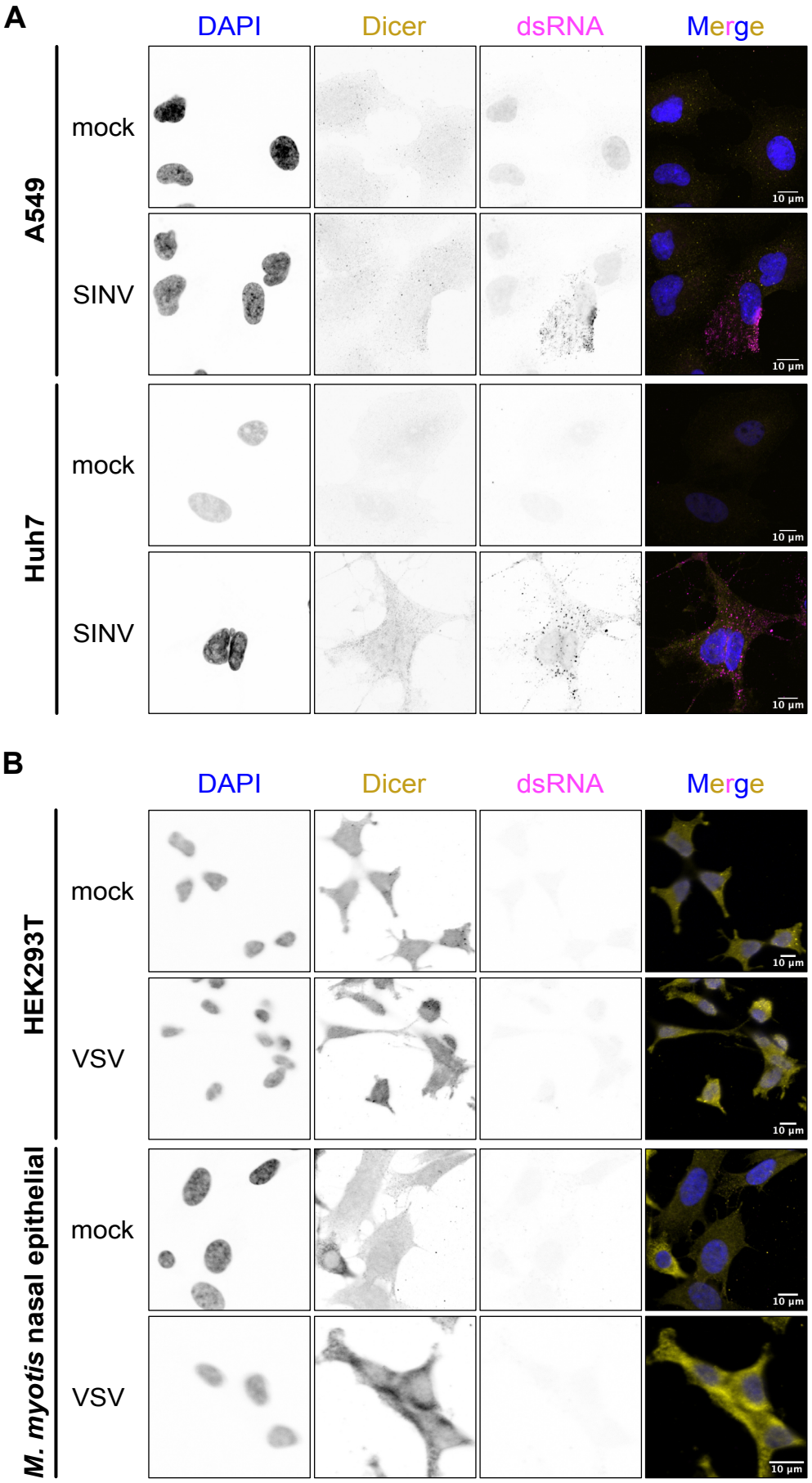
A
DAPI
Dicer
dsRNA
Merge
A549
mock
SINV
Huh7
mock
SINV
10 µm
B
DAPI
Dicer
dsRNA
Merge
HEK293T
mock
VSV
M. myotis nasal epithelial
mock
VSV
10 µm

Figure S2